Applied Catalysis A, General 540 (2017) 68–74

Contents lists available at ScienceDirect

Applied Catalysis A, General

journal homepage: www.elsevier.com/locate/apcata

Feature Article

Single-step synthesis of dimethyl ether from biomass-derived syngas over CuO-ZnO-MO_x (M = Zr, Al, Cr, Ti)/HZSM-5 hybrid catalyst: Effects of MO_x

Yuxi Hua[a], Xiaoming Guo[a,*], Dongsen Mao[a], Guanzhong Lu[a], Garry L. Rempel[b], Flora T.T. Ng[b]

[a] Research Institute of Applied Catalysis, School of Chemical and Environmental Engineering, Shanghai Institute of Technology, Shanghai 201418, PR China
[b] Department of Chemical Engineering, University of Waterloo, Waterloo N2L 3G1, Canada

ARTICLE INFO

Keywords:
Dimethyl ether
Biomass-derived syngas
Cu-Zn-based catalyst
Cu surface area
Water-gas shift reaction

ABSTRACT

A series of CuO-ZnO-MO_x (M = Zr, Al, Cr, Ti) catalysts were prepared by co-precipitation method and characterized by ICP-OES, XRD, N_2 adsorption, N_2O titration, H_2-TPR, and XPS. The CuO-ZnO-ZrO_2 catalyst exhibits the highest BET surface area and Cu surface area. For all the CuO-ZnO-MO_x catalysts, Cu^0 was the predominant copper species detectable on the surface of both reduced and spent samples. As-prepared CuO-ZnO-MO_x catalysts were mixed physically with HZSM-5 zeolite to synthesize dimethyl ether (DME) via biomass-derived syngas. The highest CO conversion and DME yield were obtained over a CuO-ZnO-ZrO_2/HZSM-5 hybrid catalyst. The CO conversion increases with the increase in the Cu surface area, but the relationship between them is not linear. Due to the H_2-deficient characteristic of biomass-derived syngas, the water-gas shift reaction, by which H_2 can be produced in-situ for the hydrogenation of CO, plays an important role in the direct DME synthesis.

1. Introduction

Dimethyl ether (DME) is an important chemical intermediate for producing some valuable chemicals such as dimethyl sulfate, methyl acetate, methyl formate and lower olefins [1–3]. Since the physical and chemical properties of DME are similar to those of liquefied petroleum gas (LPG), it also can be used as a substitute for LPG [1,2,4]. To mitigate the problem of air pollution, recently, DME has gained attention as a clean alternative fuel for diesel engines due to its lower NO_x emission, lower particulates formation and less engine noise compared with the traditional diesel fuels [5].

It is well known that DME is synthesized commercially from syngas, which could be produced via coal gasification, natural gas reforming and biomass gasification [6–9]. Considering the fast depletion of fossil fuels and the impact of global warming, the route based on biomass gasification has been the most promising technology for producing syngas because biomass is a renewable energy resource and a carbon neutral fuel [10,11]. However, quite different from fossil-based syngas, biomass-derived syngas contains much more CO_2 but less H_2 (i.e. CO_2-rich and H_2-deficient) [7,12,13].

The traditional process for DME production from syngas is a two-step process. First, methanol is produced on a Cu-based catalyst via the hydrogenation of CO or CO_2, and then DME forms over a solid acid catalyst like γ-Al_2O_3 or ZSM-5 zeolite by the dehydration of methanol [14,15]. These two steps are carried out separately in different reactors. Lately, a single-step process was proposed and developed using the hybrid catalysts (Cu-based catalysts and solid acid catalysts) in one reactor for the direct production of DME [16,17]. With the single-step process, the methanol synthesis and methanol dehydration can be performed simultaneously, and the equilibrium limitation that exists for methanol synthesis could be easily overcome by the in situ dehydration of methanol [18].

To improve the catalytic performance of the hybrid catalysts for the DME synthesis, great efforts have been made to increase the copper dispersion of Cu-based catalysts [12,19–21], tune the acidic property of solid-acid catalysts [13,22–24], balance the two active sites (active sites for methanol synthesis and dehydration) [25] and promote the synergetic effects between the metallic and acidic catalysts [26–28]. As far as the methanol synthesis components of the hybrid catalysts are concerned, ternary catalysts containing Cu, Zn and an amphoteric oxide, are usually employed [29,30]. Apart from the most common CuO-ZnO-$A1_2O_3$ catalyst, many studies using CuO-ZnO-ZrO_2 and CuO-ZnO-TiO_2 as the methanol synthesis component for DME synthesis have been reported [12,22,31–33]. Although there are a few reports investigating the influence of the tertiary component amphoteric oxide on the properties of hybrid catalysts for DME synthesis via the fossil-base syngas, corresponding work for DME synthesis from the biomass-derived syngas is absent, to the best of our knowledge.

* Corresponding author.
E-mail address: guoxiaoming@sit.edu.cn (X. Guo).

http://dx.doi.org/10.1016/j.apcata.2017.04.015
Received 31 January 2017; Received in revised form 18 April 2017; Accepted 21 April 2017
Available online 25 April 2017
0926-860X/

In this study, a series of CuO-ZnO-MO_x (M = Zr, Al, Cr, Ti) catalysts were prepared and used as the methanol synthesis component; HZSM-5 was chosen as the acidic component since it exhibited excellent performance for methanol dehydration [14,20]. These two components were then physically mixed and used for DME synthesis from biomass-derived syngas. The influence of MO_x on the properties of Cu-based catalysts and hybrid catalysts were emphasized. Also, noting the composition characteristic of biomass-derived syngas, the role of the water-gas shift reaction in the catalytic process was discussed.

2. Experimental

2.1. Catalyst preparation

The methanol synthesis component, CuO-ZnO-ZrO_2 (CZZ) catalyst with a nominal atomic ratio of Cu:Zn:Zr = 6:3:1 was prepared by a co-precipitation method. Specifically, an aqueous solution containing the respective metal nitrates ($Cu(NO_3)_2$, $Zn(NO_3)_2$, and $Zr(NO)_4$) and a Na_2CO_3 solution were simultaneously added to the deionized water at 70 °C. The resulting suspension was stirred continuously and kept at pH = 7.0 by adjusting the relative addition rates of two solutions. After complete precipitation, the obtained precipitate was aged for 1 h. Then, the precipitate was filtered off and washed repeatedly with deionized water to remove residual sodium ions. The filter cake was dried at 110 °C for 12 h and subsequently calcined at 350 °C for 4 h. The CuO-ZnO-Al_2O_3 (CZA), CuO-ZnO-Cr_2O_3 (CZC) and CuO-ZnO-TiO_2 (CZT, with $TiCl_3$ as the Titanium source) catalysts were prepared using the same procedure. HZSM-5 with a Si/Al ratio of 38 was employed as the methanol dehydration component and purchased from the catalyst plant of Nankai University (China). CuO-ZnO-MO_x (CZM) and HZSM-5 were tableted separately and pulverized into granules (40–60 mesh). The hybrid catalysts were prepared by mixing physically CuO-ZnO-MO_x and HZSM-5 with a weight ratio of 4:1. All chemicals used were of reagent grade purity purchased from Shanghai Chemical Reagent Corporation, China.

2.2. Catalysts characterization

Elemental composition of the calcined catalysts was determined by inductively coupled plasma-optical emission spectroscopy (ICP-OES), using a Thermo iCAP 6300 apparatus.

Powder X-ray diffraction (XRD) patterns of the sample were acquired on a PANalytical X'Pert instrument using Ni-filtered Cu Kα radiation at 40 kV and 40 mA. Two theta angles ranged from 20° to 60° with a speed of 6° per minute.

The BET specific area of the sample was determined by N_2 adsorption isotherms (−196 °C) on a Micrometrics ASAP–2020 M + C adsorption apparatus. The samples were evacuated at 200 °C for 6 h prior to N_2 dosage. The specific surface areas (S_{BET}) were calculated from the linear part of the Brunauer-Emmett-Teller (BET) plot.

Temperature-programmed reduction (TPR) measurements were performed in a linear quartz micro-reactor (i. d. 4 mm). 30 mg of sample was purged with N_2 at 300 °C for 1 h to remove adsorbed water and other contaminants. After cooled down to 50 °C, the catalyst was exposed to 10% H_2/N_2 (50 mL/min) at a heating rate of 5 °C/min up to 300 °C. H_2 consumption was monitored by a thermal conductivity detector.

The copper surface area (S_{Cu}) was determined by N_2O titration using a six-way valve equipped with a sample loop. About 0.2 g of sample was loaded into a linear quartz micro-reactor (i. d. 4 mm) and reduced in a 10% H_2/N_2 gas mixture at 300 °C for 1 h. After the reduction, the sample was purged with He and cooled down to the reaction temperature (60 °C). Then, a sample loop of 2 vol% N_2O/He gas mixture was intermittently fed into the reactor. The N_2 produced by the decomposition of N_2O on the exposed Cu atoms was detected using a mass spectrometer (Pfeiffer Vacuum Quadstar, 32-bit). The metallic copper surface area was calculated assuming an atomic copper surface density of 1.46×10^{19} atoms/m^2 and a stoichiometry of $N_2O/Cu = 0.5$ [34].

The X-ray photoelectron spectroscopy (XPS) and X-ray-induced Auger electron spectroscopy were recorded on an ESCALA 250 Xi spectrometer, using a standard Al K_α X-ray source (1486.6 eV). The energy analyzer was set to a pass energy of 30 eV. The binding energy (BE) values were referenced to the adventitious C 1 s peak (284.6 eV). Quantification of the surface atomic concentrations was carried out using the sensitivity factors supplied for the XPS instrument. The XPS instrument was equipped with a reaction chamber with controlled atmosphere and temperature, in which the catalyst samples could be treated under different conditions. The samples were transferred between the reaction chamber and analysis chamber by a transfer rod under ultrahigh vacuum.

NH_3-TPD experiments for the surface acidity determination were performed using a conventional flow apparatus equipped with a thermal conductivity detector. In a typical analysis, 100 mg of the sample was loaded into a linear quartz micro-reactor and pretreated in a 10% H_2/N_2 gas mixture at 300 °C for 1 h. The sample was cooled down to 50 °C and then exposed to NH_3 for 30 min. Then, the sample was purged with N_2 at 100 °C for 1 h to remove the physisorbed NH_3. The TPD measurements were conducted in flowing N_2 (30 ml/min) from 100 to 550 °C with a constant heating rate of 10 °C/min.

2.3. Catalytic activity measurement

The catalytic activity test was performed in a continuous-flow, fixed-bed reactor. Typically, 0.5 g of catalyst diluted with quartz sand (both in 40–60 mesh) was packed into a stainless steel tubular reactor (5 mm i. d.). Prior to each test, the catalyst was reduced in-situ in a 10% H_2/N_2 stream (30 mL/min) at 300 °C for 3 h under atmospheric pressure. Then, the reactor was cooled to 160 °C, and the biomass-derived syngas ($H_2/CO/CO_2/N_2$ = 36/36/18/10, molar) was introduced, raising the pressure to 3.0 MPa and the temperature to a given temperature. All post-reactor lines and valves were heated to 150 °C to prevent product condensation. The product stream was analyzed by an online-GC (7820A, Agilent) equipped with a TCD (for CO, CO_2, and CH_4 analysis) and a FID (for DME, methanol, and other hydrocarbons analysis). The CO and CO_2 conversion, product selectivity and DME yield were calculated using the formula given in Ref [19].

3. Results and discussion

3.1. Structural and textural properties

The chemical compositions of the calcined CZM catalysts determined by ICP-OES are presented in Table 1. The compositions of CZM catalysts generally agree with the nominal compositions calculated for catalyst preparation, and a ratio of Cu/Zn is about 2.1 for all samples.

The XRD patterns of the calcined CZM catalysts were collected and presented in Fig. 1(a). The diffraction peaks at 2θ of 35.6°, 38.8° are identified as CuO phase (PDF #48-1548), and the diffraction peaks at 31.7°, 34 .5°, 36.2°, 47.5° and 56.6°are assigned to the phase of ZnO (PDF #36-1451). There is no distinct diffraction peak of MO_x (M = Zr, Al, Cr and Ti) crystallite for the corresponding catalyst. This indicates

Table 1
Chemical composition of the calcined CZM catalysts.

Catalyst	Metal content (mol %)			Cu/Zn atomic ratio
	Cu	Zn	M	
CZZ	61.3	29.8	Zr: 8.9	2.06
CZA	60.6	28.6	Al: 10.8	2.12
CZC	61.9	29.6	Cr: 8.5	2.09
CZT	59.9	28.8	Ti: 11.3	2.08

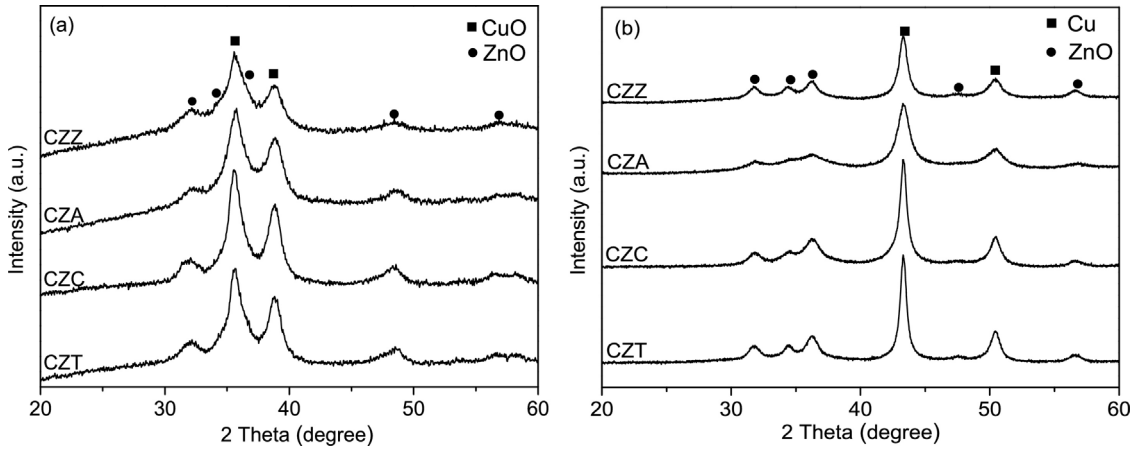

Fig. 1. XRD patterns of CZM catalysts: (a) calcined catalysts, (b) reduced catalysts.

Table 2
Physicochemical properties of CZM catalysts.

Catalyst	BET surface area (m^2/g)	Cu surface area[a] (m^2/g)	CuO crystallite size[b] (nm)	Cu crystallite size[b] (nm)	D_{Cu}[c] (%)	S_{Cu}/S_{BET} (%)
CZZ	104.2	7.0	5.0	10.8	2.39	6.7
CZA	77.2	5.9	5.4	11.2	1.84	7.6
CZC	75.8	5.2	6.4	13.2	1.68	6.9
CZT	90.6	4.4	6.8	14.2	1.42	4.8

[a] Determined by N_2O titration method.
[b] Calculated with Scherrer equation using the most intense peaks centered at 35.6° and 43.3° for CuO and Cu, respectively.
[c] Derived from N_2O titration measurements.

that MO_x exists in an amorphous form or a low degree of crystallization. The average crystallite size of CuO was calculated using the Scherrer equation, and it decreased in the order of CZT > CZC > CZA > CZZ. In comparison with Al_2O_3, Cr_2O_3 and TiO_2, ZrO_2 enhanced the dispersion of CuO. Fig. 1(b) shows the XRD patterns of the reduced CZM catalysts. The characteristic peaks of the cubic metallic Cu were observed at 2θ = 43.5 and 50.4 for all the CZM samples, suggesting that CuO in the catalyst was converted to Cu after reduction. No apparent change is observed for the characteristic XRD peaks of ZnO. The crystallite size of Cu in the reduced catalysts was also estimated. As shown in Table 2, the particle size of Cu is larger than that of the corresponding CuO in the calcined samples. This is because the reduction of CuO with H_2 is an exothermic reaction, which results in a coalescence of metallic copper particles [35]. In addition, the order of the crystallite size of Cu is the same as that of CuO in the calcined catalysts.

The BET surface areas (S_{BET}) of the catalysts are listed in Table 2. A maximum S_{BET} of 104.2 m^2/g is obtained for the CZZ sample, whereas a minimum of 75.8 m^2/g is observed for the CZC catalyst. The metallic copper surface area (S_{Cu}), as determined by the N_2O titration technique, is also shown in Table 2. The value of S_{Cu} decreases in the order CZZ > CZA > CZC > CZT, and the dispersion of Cu exhibits the same trend. This result is in good agreement with the results of XRD since a smaller CuO particle size corresponds to a higher copper surface area. Moreover, the ratios of S_{Cu}/S_{BET} for the catalysts were calculated, and a minimum value was obtained for the CZT sample, suggesting that TiO_2 is least capable to help the dispersion of Cu compared to ZrO_2, Al_2O_3, and Cr_2O_3 under the condition where the same BET surface area is available.

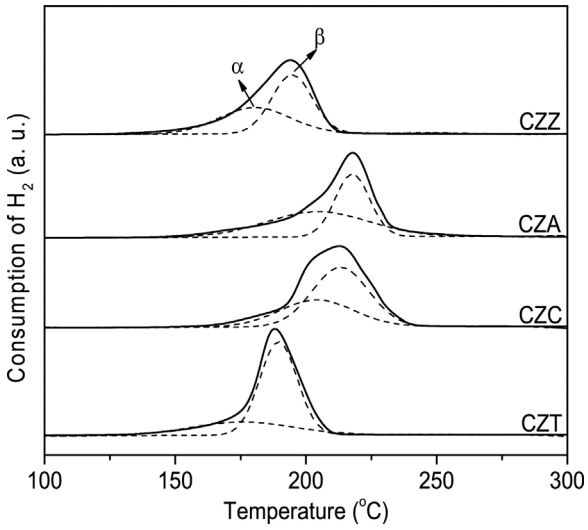

Fig. 2. TPR profiles of CZM catalysts.

3.2. The reducibility of catalyst

In order to investigate the reduction behavior of the CZM catalysts, TPR measurements were carried out. As shown in Fig. 2, the reduction profiles of all samples exhibit an asymmetric reduction peak in the range of 150–250 °C, which can be deconvoluted into two Gaussian peaks. The low temperature peak (α peak) is related to the reduction of highly dispersed CuO, whereas the high temperature peak (β peak) is due to the reduction of bulk CuO [31,36]. The peak positions and their contributions are summarized in Table 3. Generally, the reduction temperature of CuO in the catalyst is affected by the particle size of CuO and the interaction between CuO and other components [30,37]. The smaller the CuO particle is, the lower the reduction temperature is expected. In this study, comparing with the CuO species in CZA and CZC samples, CuO in CZZ and CZT catalysts are reduced at a lower

Table 3
Temperature of reduction peaks and their contribution to the H_2-TPR profiles of CZM catalysts.

Catalyst	Peak α		Peak β	
	T (°C)	Fraction (%)	T (°C)	Fraction (%)
CZZ	180	43.8	194	56.2
CZA	204	54.3	217	45.7
CZC	204	37.3	213	62.7
CZT	175	27.7	189	72.3

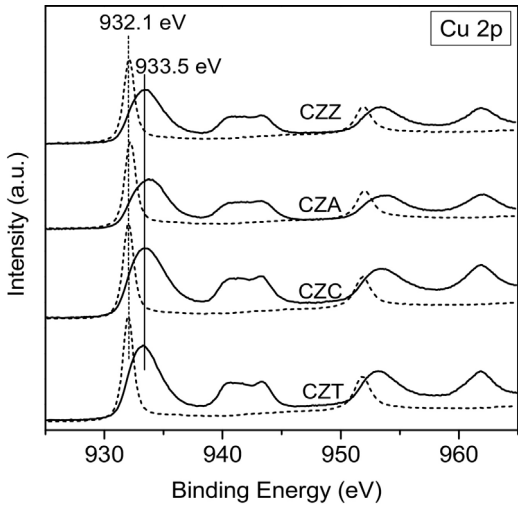

Fig. 3. Cu 2p XPS for CZM catalyst: fresh sample after calcination in air (solid) and sample after reduction in H_2 (dash).

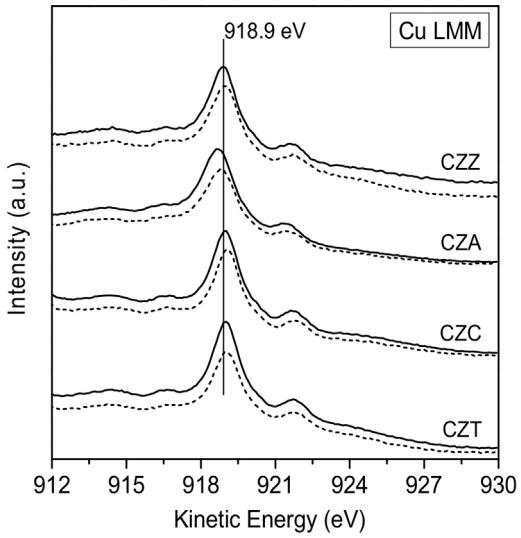

Fig. 4. Cu(LMM) AES for the CZM catalyst: sample after reduction in H_2 (solid) and sample after exposure to the feed gas (dash).

temperature. Obviously, the order of the reduction temperature of the investigated catalysts is not consistent with that of the particle size of CuO, as shown in the XRD results. Therefore, it can be inferred that the interaction between CuO and MO_x plays an important role in determining the reduction temperature. Noting that the valence of Zr and Ti cations is +4 while Al and Cr are in a +3 oxidation state, it is possible that the interaction between CuO and the tetravalent cations is more favorable for the reduction of CuO species [38]. In addition, the relative contribution of the α peak to the TPR pattern of the CZT catalyst is only 27.7%, although the CZT catalyst exhibits the lowest reduction temperature.

3.3. Chemical state and composition on the surface of catalyst

The chemical states and compositions on the catalyst surface were investigated using a XPS technique under three different conditions: (1) after calcination in air, (2) after reduction in 10% H_2/N_2 at 300 °C for 1 h, and (3) after exposure to the feed gas at 250 °C for 1 h. The XPS of the Cu 2p for the calcined catalysts are illustrated in Fig. 3. The Cu 2p3/2 peak locates at a binding energy (BE) in the range 933.4–933.8 eV together with an intense shakeup satellite peak at about 942.0 eV for all the catalysts, which is characteristic of Cu^{2+} [39,40]. The small difference in the BE value among the four samples suggests that the influence of MO_x on the chemical state of Cu is not appreciable. As shown in Fig. 3, after in-situ reduction with hydrogen, the shakeup feature disappeared and the BE of Cu 2p3/2 shifted to 932.1 eV, indicating that Cu^{2+} had been reduced completely. Since the BE values of Cu 2p3/2 core electrons for Cu^0 and Cu^+ are almost identical, it is difficult to differentiate between these two species. Fortunately, the kinetic energies (KE) of LMM Auger electrons for Cu^0 (918.8 eV) and Cu^+ (916.8 eV) are separated by approximately 2.0 eV, which allows to distinguish the oxidation state of copper. In this study, the X-ray-induced Auger electron spectroscopy of the reduced catalysts were collected and presented in Fig. 4. All catalysts displayed the Cu (LMM) Auger peaks centered between 918.7 and 919.0 eV, demonstrating that Cu^0 is the predominant copper species detectable on the surface of the reduced catalyst. Further exposure to the feed gas at 250 °C for 1 h, there is no significant change in the Auger peaks for all the investigated catalysts, as shown in Fig. 4. The result discloses that copper remains in the metallic state (Cu^0) under the reaction conditions in this case. It is worth to mention here that, for the copper-based methanol synthesis catalysts, the valence of Cu active site has been a long-standing controversy. Some authors reported that Cu^+ species was detected over the surface of Cu-based catalysts besides Cu^0 [13,20], but others demonstrated that Cu^0 was the only active site [41–44]. Clearly, the results of our experiments support the latter view. The presence of Cu^+ in some cases maybe originated from the unintentional exposure to air during the transfer from a reactor to the analysis chamber of XPS instrument [42,44].

The relative surface concentration of metal and the Cu/Zn ratio, as estimated from the peak area and atomic sensitivity factors, are presented in Table 4. For the calcined samples, the concentration of Cu on the surface is lower than that in the bulk phase (as shown in Table 1), whereas a phenomenon of surface Zn-enrichment is observed. Consequently, the surface Cu/Zn ratios decrease markedly comparing to the bulk values (~2.1) of the catalysts. Similar results have been reported extensively [45,46]. After the reduction or reaction treatment, the depletion of Cu and enrichment of Zn appears to be more pronounced. For example, the surface Cu/Zn ratios of CZZ decrease to 0.81 and 0.55 after the reduction and reaction treatment, respectively. This result suggests that the surface Cu is partly substituted by Zn because Cu and Zn atoms can migrate during the reduction and reaction treatment [45]. In other word, a surface reconstruction took place. It is notable that the surface concentration of Al in CZA is much higher than those of Zr, Cr and Ti in the corresponding catalysts. Similar results have been reported by Li et al. [47], and they ascribe the reason to the higher lattice energy of Al, which will hinder the Al migration during the preparation, reduction and reaction process.

3.4. Surface acidity of the hybrid catalysts

The strength and amount of acid sites on the hybrid catalysts were determined using the NH_3-TPD technique. As shown in Fig. 5, a typical NH_3-TPD profile with two desorption peaks, corresponding to NH_3 desorbed from the weak and strong acid sites respectively, was observed on the pure zeolite HZSM-5 [22]. After mixing with the CZM components, the high temperature desorption peaks for the hybrid CZM/HZSM-5 catalysts shift slightly to lower temperature compared to the pure zeolite HZSM-5, indicating that the strength of strong acid site becomes weak. This result suggests that the acidity of HZSM-5 is somewhat affected by CZM components although CZM and HZSM-5 are pre-pelletized separately before mixing. Similar observations have also been reported previously by other researchers [26]. The amount of acid sites is listed in Table 5, and the largest amount of strong acid sites was obtained over the CZC/HZSM-5 sample.

Table 4
Relative surface concentration of metal (atomic%) for CZM catalysts subjected to different treatments.

Catalyst	After calcination				After reduction				After exposure to feed gas			
	Cu	Zn	M	Cu/Zn	Cu	Zn	M	Cu/Zn	Cu	Zn	M	Cu/Zn
CZZ	52.3	37.9	9.8	1.38	39.8	49.4	10.8	0.81	31.5	57.6	10.9	0.55
CZA	41.5	30.2	28.3	1.37	31.3	30.3	38.4	1.03	29.5	32.3	38.3	0.91
CZC	44.2	44.6	11.2	0.99	34.8	52.0	13.2	0.67	32.3	52.1	15.6	0.62
CZT	50.6	42.7	6.7	1.18	36.6	55.3	8.1	0.66	33.0	58.5	8.6	0.56

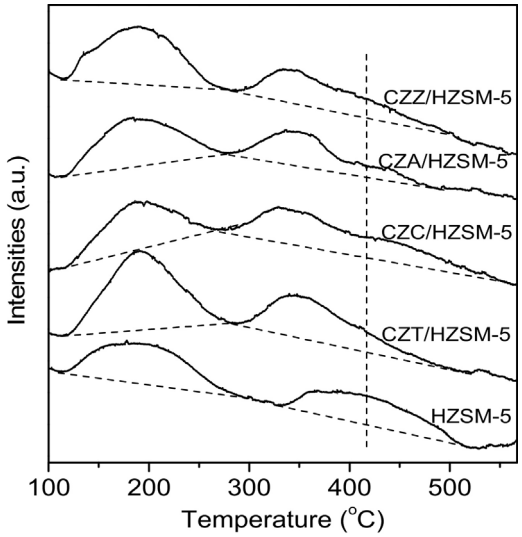

Fig. 5. NH_3-TPD patterns of CZM/HZSM-5 catalysts.

Table 5
NH_3 desorption properties of the hybrid catalysts.

Catalyst	Amount of acid sites (mmol/g_{HZSM-5})		
	Weak	Strong	Total
CZZ/HZSM-5	1.22	0.79	2.01
CZA/HZSM-5	1.02	0.68	1.70
CZC/HZSM-5	0.94	1.15	2.09
CZT/HZSM-5	1.52	0.96	2.48
HZSM-5	0.94	0.80	1.75

3.5. Catalytic performance

There are four reactions involved in DME synthesis from biomass-derived syngas. The equilibria can be described as:

Methanol synthesis: $CO + 2H_2 = CH_3OH\ \Delta H_{298} = -90.6\ kJ/mol$ (1)

$CO_2 + 3H_2 = CH_3OH + H_2O\ \Delta H_{298} = -49.47\ kJ/mol$ (2)

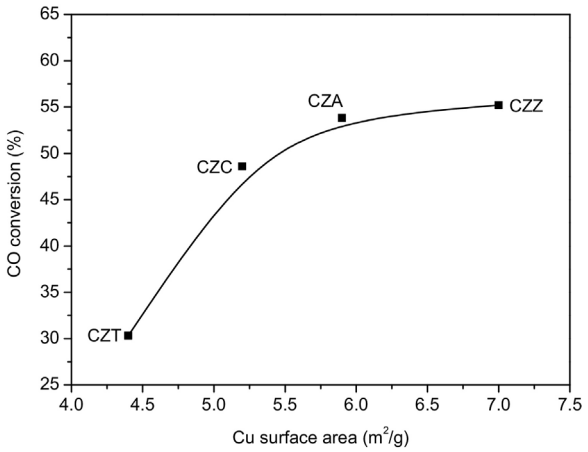

Fig. 6. Relationship between the CO conversion and Cu surface area. Reaction conditions: $H_2/CO/CO_2/N_2$ = 36/36/18/10 (molar ratio), T = 250 °C, P = 3.0 MPa, GHSV = 4800 h^{-1}.

Methanol dehydration: $2CH_3OH = CH_3OCH_3 + H_2O\ \Delta H_{298} = -23.4\ kJ/mol$ (3)

Water-gas shift (WGS) reaction: $CO + H_2O = H_2 + CO_2\ \Delta H_{298} = -41.2\ kJ/mol$ (4)

Methanol is produced via CO and CO_2 hydrogenation (reaction (1) and (2)) on Cu-based catalysts, followed by in-situ dehydration of methanol (reaction (3)) to form DME over solid-acid catalyst. Since the Cu-based catalyst is also active for WGS reaction (4) [48,49], the mutual transformation between CO and CO_2 is easy to realize.

The catalytic data for DME synthesis from biomass-derived syngas on CuO-ZnO-MO_x/HZSM-5 hybrid catalysts are summarized in Table 6. Under the present reaction conditions, the major products are DME, methanol, CO_2 and light hydrocarbons. The highest CO conversion and DME yield were obtained over the CZZ/HZSM-5 catalyst, followed successively by CZA/HZSM-5, CZC/HZSM-5 and CZT/HZSM-5. Except for the sample of CZC/HZSM-5, the value of DME selectivity is about 61% for the investigated samples. The methanol selectivity is low for all the catalysts, ranging from 3.0 to 4.2%, which indicates that the active site for dehydration on the solid-acid catalyst is sufficient to convert methanol to DME. For the hydrocarbon selectivity, a maximum of 7.4%

Table 6
Catalytic properties of CZM/HZSM-5 catalysts.

Catalyst	Conversion (%)		Selectivity (%)				DME Yield (%)	$TOF_{CO} \times 10^3$ (s^{-1})
	CO	CO_2	DME	CH_3OH	CO_2	hydrocarbons		
CZZ/HZSM-5	55.2	−35.7	61.4	3.0	32.8	2.8	33.9	21.1
CZA/HZSM-5	53.8	−34.9	61.8	3.5	32.6	2.1	33.2	28.7
CZC/HZSM-5	48.6	−32.8	55.8	3.2	33.6	7.4	27.1	28.0
CZT/HZSM-5	30.3	−18.7	60.5	4.2	31.0	4.3	18.3	24.2

Reaction conditions: $H_2/CO/CO_2/N_2$ = 36/36/18/10 (molar ratio), T = 250 °C, P = 3.0 MPa, GHSV = 4800 h^{-1}. The CO_2 selectivity refers to the fraction of CO_2 produced in-situ during the catalytic reaction. Hydrocarbons include CH_4 and a small amount of C_2 hydrocarbons.

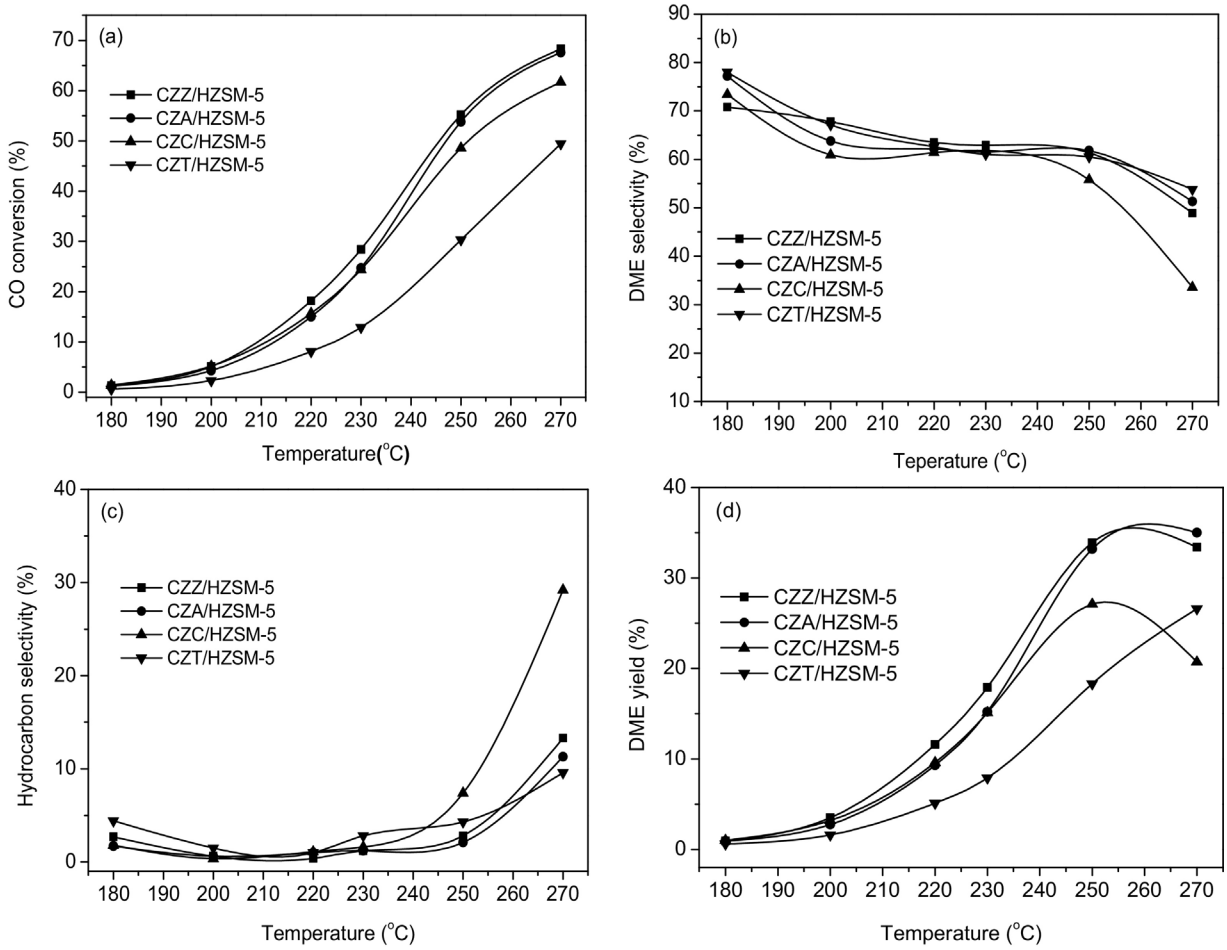

Fig. 7. Effects of reaction temperature on the catalytic performance of CZM/HZSM-5 catalysts: (a) CO conversion; (b) STY of DME; (c) Hydrocarbons selectivity; (d) DME selectivity. Reaction conditions: $H_2/CO/CO_2/N_2$ = 36/36/18/10 (molar ratio), P = 3.0 MPa, GHSV = 4800 h^{-1}.

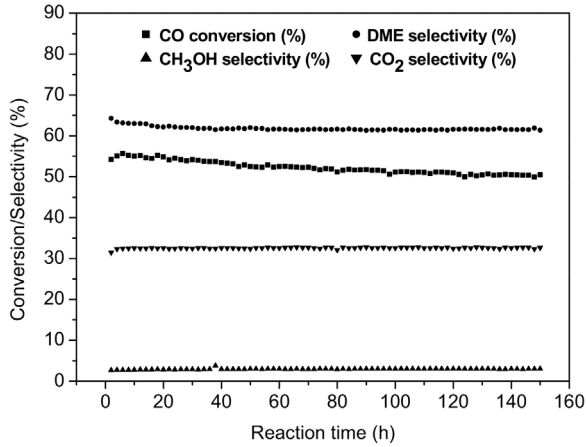

Fig. 8. Long-term test of activity and selectivity of the CZZ/HZSM-5 catalyst. Reaction conditions: $H_2/CO/CO_2/N_2$ = 36/36/18/10 (molar ratio), T = 250 °C, P = 3.0 MPa, GHSV = 4800 h^{-1}.

was observed on CZC/HZSM-5. It is well known that strong acidic sites promote the generation of secondary products like hydrocarbons, resulting in a low selectivity for DME [22]. Thus, the highest hydrocarbons selectivity and lowest DME selectivity are ascribed to the high content of strong acid sites over CZC/HZSM-5, as shown in Section 3.4.

It can be seen from Table 6 that CO_2 conversions were negative for all investigated samples. As stated above, CO_2 is consumed via reaction (2) to form methanol and is produced simultaneously via the WGS reaction. A large negative value of CO_2 conversion suggests that the amount of CO_2 generated via WGS reaction was much higher than that consumed in reaction (2), and similar results were reported by Song et. al [19]. In other words, CO_2 hydrogenation to methanol is negligible due to the H_2-deficient conditions. For this reason, CO_2 is treated simply as a product in the literature [12] although a high concentration of CO_2 is presented in the feed gas. In this study, as Table 6 shows, the selectivity of CO_2 produced in-situ is around 32% for all the samples when CO_2 is treated as a product. It is noteworthy that, accompanied with the production of CO_2 via the WGS reaction, a large amount of H_2 is formed in-situ. Compared with the fossil-based syngas with a H_2/CO ratio of 2, the biomass-derived syngas is characterized as a low H_2/CO ratio (close or below to 1). Therefore, the WGS reaction is particularly important in the single-step synthesis of DME from biomass-derived syngas because a hydrogen-rich environment, which is favorable for obtaining a high CO conversion, can be created via the WGS reaction. Moreover, the DME selectivity decreases since a large amount of CO_2 is produced via WGS reaction.

As mentioned above, both CO hydrogenation and the WGS reactions occur on the Cu-based catalyst. Therefore, the total CO conversion via CO hydrogenation and the WGS reaction depends on the number and intrinsic activity of Cu sites. A plot of CO conversion versus the copper surface area (S_{Cu}), which is a reflection of the number of Cu sites, is presented in Fig. 6. It can be seen that the CO conversion increases with the increase in the S_{Cu}, but the rate of increase slows down gradually. The nonlinear relationship between CO conversion and the S_{Cu} indicated that the intrinsic activities of Cu sites in the investigated CuO-ZnO-MO_x catalysts are different. To further disclose the relation-

ship between CO conversion and S_{Cu}, the turnover frequency (TOF) of CO conversion, which represents the molecule number of CO converted per second per metallic copper atom, was calculated. As Table 6 shown, the value of TOF varies in the range of 21.1–28.7 $\times 10^{-3}\,s^{-1}$. The TOF value should be a constant if the intrinsic activity of Cu site is equivalent [31,50]. In this study, the difference in the intrinsic activity of Cu site can be mainly ascribed to two factors. One is the interaction between CuO and MO_x, which affects the intrinsic activity of Cu site [30]. The interaction between CuO and Al_2O_3 (or Cr_2O_3) is more favorable for the CO conversion leading to a higher TOF over the CZA (or CZC) sample. The other one is related to the structure-sensitive character of the CO hydrogenation (or WGS reaction) over the Cu-based catalyst. The structure-sensitive character means that the intrinsic activity of Cu site is affected by the particle size of Cu [50]. Furthermore, since the methanol dehydration to DME occurs at a faster rate than CO hydrogenation to methanol [19], the obtained DME yield over different CZM/HZSM-5 hybrid catalysts coincide with the variation of CO conversion.

The effects of reaction temperature on the catalytic performances of CZM/HZSM-5 hybrid catalysts were investigated, and the results are presented in Fig. 7. The conversion of CO increases as the temperature increases from 180 to 270 °C (Fig. 7(a)), revealing that the reaction is still far from equilibrium [51]. The selectivity of DME and light hydrocarbons goes through smoothly from 180 to 250 °C. However, as the temperature reaches 270 °C, an obvious decrease in DME selectivity was observed along with a remarkable increase in the selectivity of light hydrocarbons (Fig. 7(b) and (c)). This is because DME will be further dehydrated and polymerized to light hydrocarbons at a high temperature [8]. For the DME yield, with the elevation of temperature, it increases first and then decreases, and a maximum is obtained at 250 °C (Fig. 7(d)).

The stability of the most efficient CZZ/HZSM-5 catalyst for single-step synthesis of DME from biomass-derived syngas was measured over a 150-h period, in which the reactor was operated continuously under the test conditions. As shown in Fig. 8, the CO conversion decreases slightly by 6% from its initially stabilized values during the first 80 h, and then it remains stable. The small decrease in CO conversion is mainly ascribed to the deactivation of the methanol synthesis catalyst [52,53]. As for the selectivity of products, no obvious change can be found during the whole test period.

4. Conclusions

MO_x (M = Zr, Al, Cr, Ti) significantly affects the physicochemical properties of CuO-ZnO-MO_x catalysts and further the catalytic performances of the hybrid catalysts CuO-ZnO-MO_x/HZSM-5 for the single-step synthesis of DME from biomass-derived syngas. The highest BET surface areas and Cu surface areas were obtained on CuO-ZnO-ZrO_2 sample. The reduction temperature of CuO is affected by the interaction between CuO and MO_x, and a lower reduction temperature is observed on CuO-ZnO-ZrO_2 and CuO-ZnO-TiO_2. Only Cu^0 species was detectable on the surface of the catalysts after exposing them to a reductive atmosphere and biomass-derived syngas. The acidity of HZSM-5 changes slightly after the mixing process with the CZM components. The catalytic activity decreases in the order CZZ/HZSM–5 > CZA/HZSM–5 > CZC/HZSM–5 > CZT/HZSM-5. The CO conversion increases with the increase in the Cu surface area, but the relationship between them is not linear. A negative conversion of CO_2 was observed for all samples because a large amount of CO_2 was produced via the WGS reaction accompanied with the formation of hydrogen.

Acknowledgements

The authors thank Shanghai Municipal Education Commission (International Visiting Scholar Program, No. 2014-56), Shanghai Municipal Science and Technology Commission (No. 13ZR1441200, No. 13ZR1461900) and the National Natural Science Foundation of China (No. 21273150) for financial support.

References

[1] C. Arcoumanis, C. Bae, R. Crookes, E. Kinoshita, Fuel 87 (2008) 1014–1030.
[2] G.Y. Cai, Z.M. Liu, R.M. Shi, C.Q. He, L.X. Yang, C.L. Sun, Y.J. Chang, Appl. Catal. A: Gen. 125 (1995) 29–38.
[3] K.P. Sun, W.W. Lu, M. Wang, X.L. Xu, Catal. Commun. 5 (2004) 367–370.
[4] Q.J. Ge, Y.M. Huang, F.Y. Qiu, S.B. Li, Appl. Catal. A: Gen. 167 (1998) 23–30.
[5] T.A. Semelsberger, R.L. Borup, H.L. Greene, J. Power Sources 156 (2006) 497–511.
[6] A.V. Bridgwater, Chem. Eng. J. 91 (2003) 87–102.
[7] X.L. Yin, D.Y.C. Leung, J. Chang, J.F. Wang, Y. Fu, C.Z. Wu, Energy Fuels 19 (2005) 305–310.
[8] Y.P. Li, T.J. Wang, X.L. Yin, C.Z. Wu, L.L. Ma, H.B. Li, L. Sun, Fuel 88 (2009) 2181–2187.
[9] A.A. Iordanidis, P.N. Kechagiopoulos, S.S. Voutetakis, A.A. Lemonidou, I.A. Vasalos, Int. J. Hydrog. Energy 31 (2006) 1058–1065.
[10] C.N. Hamelinck, A.P.C. Faaij, J. Power Sources 111 (2002) 1–22.
[11] J. Chang, Y. Fu, Z.Y. Luo, Biomass Bioenergy 39 (2012) 67–72.
[12] J.W. Jung, Y.J. Lee, S.H. Um, P.J. Yoo, D.H. Lee, K.W. Jun, J.W. Bae, Appl. Catal. B: Environ. 126 (2012) 1–8.
[13] J.W. Bae, S.H. Kang, Y.J. Lee, K.W. Jun, J. Ind. Eng. Chem. 15 (2009) 566–572.
[14] W.H. Chen, B.J. Lin, H.M. Lee, M.H. Huang, Appl. Energy 98 (2012) 92–101.
[15] Y.Y. Zhu, S.R. Wang, X.L. Ge, Q. Liu, Z.Y. Luo, K.F. Cen, Fuel Process. Technol. 91 (2010) 424–429.
[16] J. Topp-Jorgensen, US Patent 4, 536, 485, (1985) to Haldor Topsoe A/S, Denmark.
[17] J.B. Hansen, F.H. Joensen, H.F.A. Topsoe, US Patent 5, 189, 203, (1993) to Haldor Topsoe A/S, Denmark.
[18] J. Ereña, I. Sierra, A.T. Aguayo, A. Ateka, M. Olazar, J. Bilbao, Chem. Eng. J. 174 (2011) 660–667.
[19] F.E. Song, Y.S. Tan, H.J. Xie, Q.D. Zhang, Y.Z. Han, Fuel Process. Technol. 126 (2014) 88–94.
[20] M.H. Zhang, Z.M. Liu, G.D. Lin, H.B. Zhang, Appl. Catal. A: Gen. 451 (2013) 28–35.
[21] W.G. Gao, H. Wang, Y.H. Wang, W. Guo, M.Y. Jia, J. Rare Earths 31 (2013) 470–476.
[22] D.S. Mao, W.M. Yang, J.C. Xia, B. Zhang, Q.Y. Song, Q.L. Chen, J. Catal. 230 (2005) 140–149.
[23] J.C. Xia, D.S. Mao, B. Zhang, Q.L. Chen, Y. Tang, Catal. Lett. 98 (2004) 235–240.
[24] D.F. Jin, B. Zhu, Z.Y. Hou, J.H. Fei, H. Lou, X.M. Zheng, Fuel 86 (2007) 2707–2713.
[25] R.F. Nie, H. Lei, S.Y. Pan, L.N. Wang, J.H. Fei, Z.Y. Hou, Fuel 96 (2012) 419–425.
[26] G. Bonura, M. Cordaro, L. Spadaro, C. Cannilla, F. Arena, F. Frusteri, Appl. Catal. B: Environ. 140–141 (2013) 16–24.
[27] A. García-Trenco, A. Vidal-Moya, A. Martínez, Catal. Today 179 (2012) 43–51.
[28] G.H. Yang, N. Tsubaki, J. Shamoto, Y. Yoneyama, Y. Zhang, J. Am. Chem. Soc. 132 (2010) 8129–8136.
[29] I. Melián-Cabrera, M. López Granados, J.L.G. Fierro, J. Catal. 210 (2002) 273–284.
[30] C.H. Liu, X.M. Guo, Q.S. Guo, D.S. Mao, J. Yu, G.Z. Lu, J. Mol. Catal. A: Chem. 425 (2016) 86–93.
[31] X.M. Guo, D.S. Mao, G.Z. Lu, S. Wang, G.S. Wu, J. Catal. 271 (2010) 178–185.
[32] F. Arena, K. Barbera, G. Italiano, G. Bonura, L. Spadaro, F. Frusteri, J. Catal. 249 (2007) 185–194.
[33] J. Xiao, D.S. Mao, X.M. Guo, J. Yu, Energy Technol. 3 (2015) 32–39.
[34] J. Słoczyński, R. Grabowski, A. Kozłowska, P. Olszewski, J. Stoch, J. Skrzypek, M. Lachowska, Appl. Catal. A: Gen. 278 (2004) 11–23.
[35] S.I. Fujita, S. Moribe, Y. Kanamori, M. Kakudate, N. Takezawa, Appl. Catal. A: Gen. 207 (2001) 121–128.
[36] G. Avgouropoulos, T. Ioannides, H. Matralis, Appl. Catal. B: Environ. 56 (2005) 87–93.
[37] G.R. Moradi, S. Nosrati, F. Yaripor, Catal. Commun. 8 (2007) 598–606.
[38] J. Agrell, H. Birgersson, M. Boutonnet, I. Melián-Cabrera, R.M. Navarro, J.L.G. Fierro, J. Catal. 219 (2003) 389–403.
[39] X.M. Guo, D.S. Mao, G.Z. Lu, S. Wang, G.S. Wu, J. Mol. Catal. A: Chem. 345 (2011) 60–68.
[40] L.C. Wang, Q. Liu, M. Chen, Y.M. Liu, Y. Gao, H.Y. He, K.N. Fan, J. Phys. Chem. C 111 (2007) 16549–16557.
[41] S. Natesakhawat, J. Lekse, J. Baltrus, P.R. Ohodnicki, B. Howard, X. Deng, C. Matranga, ACS Catal. 2 (2012) 1667–1676.
[42] J. Yoshihara, S.C. Parker, A. Schafer, C.T. Campbell, Catal. Lett. 31 (1995) 313–324.
[43] J. Yoshihara, C.T. Campbell, J. Catal. 161 (1996) 776–782.
[44] B. Peplinski, W.E.S. Unger, Appl. Surf. Sci. 62 (1992) 115–129.
[45] W.L. Dai, Q. Sun, J.F. Deng, D. Wu, Y.H. Sun, Appl. Surf. Sci. 177 (2001) 172–179.
[46] J. Słoczyński, R. Grabowski, P. Olszewski, A. Kozłowska, J. Stoch, M. Lachowska, J. Skrzypek, Appl. Catal. A: Gen. 310 (2006) 127–137.
[47] Z.H. Li, W. Huang, Z.J. Zuo, Y.J. Song, K.C. Xie, Chin. J. Catal. 30 (2009) 171–177.
[48] N. Schumacher, A. Boisen, S. Dahl, A.A. Gokhale, S. Kandoi, L.C. Grabow, J.A. Dumesic, M. Mavrikakis, I. Chorkendorff, J. Catal. 229 (2005) 265–275.
[49] L.G. Wang, D.R. Fang, X.Y. Huang, S.G. Zhang, Y. Qi, Z.M. Liu, J. Nat. Gas Chem. 15 (2006) 38–44.
[50] M. Boudart, Chem. Rev. 95 (1995) 661–666.
[51] S. Asthana, C. Samanta, A. Bhaumik, B. Banerjee, R.K. Voolapalli, B. Saha, J. Catal. 334 (2016) 89–101.
[52] Y.S. Luan, H.Y. Xu, C.Y. Yu, W.Z. Li, S.F. Hou, Catal. Lett. 115 (2007) 23–26.
[53] F.S.R. Barbosa, V.S.O. Ruiz, J.L.F. Monteiro, R.R.D. Avillez, L.E.P. Borges, L.G. Appel, Catal. Lett. 126 (2008) 173–178.